Effective energy controls on flocculation under various wave-current regimes

Rafael Ramírez-Mendoza[a,b], Alejandro J. Souza[b], Laurent O. Amoudry[b], Andrew J. Plater[c]

[a] *CICESE, Carr. Eda.-Tij. No. 3918, Playitas, Eda., BC, 22860, México*
[b] *National Oceanography Centre*
6 Brownlow Street, Josehp Proudman Building, Liverpool, United Kingdom, L3 5DA
[c] *Department of Geography, University of Liverpool*
Roxby Building, L69 7ZT, UK

Abstract

Transport of sediments is a critical process in the coastal zone because of its relation with coastal erosion, productivity and pollution. Of particular interest are the dynamics of suspended cohesive sediments, known as flocs, which can aggregate and break-up during the flocculation process. This changes their size, density, settling velocity and overall transport. Even though turbulence is widely accepted to be an important control on floc aggregation and break-up, specific and detailed floc behaviour is still not fully understood. The present study seeks to help in the understanding of the intra-tidal turbulence-induced flocculation under different current-wave regimes. Observations of floc size and currents at high sample rates are used to investigate the changes throughout a fortnightly cycle. The occurrence of waves at different stages during the sampling period enabled determination of three regimes of currents dominant, combined waves and currents, and wave dominant. The first two regimes showed quarter-diurnal floc size variability with aggregation during low turbulence (slack waters) and higher

Email address: rrmenz@noc.ac.uk rrafael@cicese.mx (Rafael Ramírez-Mendoza)

floc aggregation magnitude on low water slack. Break-up occurred with high turbulence (flood and ebb) with higher magnitude after ebb. During the "currents-waves" regime, waves were tidally modulated and led to enhanced aggregation and break-up, with larger floc size range than during the "current dominant" regime. Wave tidal modulation and quarter-diurnal variability of floc size were lost when waves were dominant. Flocs sizes exhibited a low range related to wave height. Inverse relationships between turbulent properties and median floc size were found for the three regimes, with higher scatter of data for the Kolmogorov microscale and shear rate due to different floc behaviour during flood and ebb phases. Effective kinetic energy obtained from the combined effect of both currents and waves seems to have a better relationship with floc size, which suggests its use as a floc size predictor instead of shear stress.
Keywords:
Flocculation, turbulence, waves, currents, sediments

1. Introduction

The dynamics of suspended sediment play an important role in estuarine systems as they are strongly related to accretion, erosion, estuarine turbidity maxima, primary productivity, pollution and overall estuarine budgets. A key characteristic of estuarine sediments is the presence of fine cohesive sediments, which may aggregate or break-up via the so-called flocculation process. The resulting suspended particulate aggregates, known as flocs, display time and space varying characteristics, such as size, density, and settling velocity and therefore influence the overall estuarine sediment transport

(Winterwerp and van Kesteren, 2004). Knowledge of the physical processes that control flocculation is crucial toward good management, sustainability of the resources, and conservation of natural ecosystems where fine sediments are important.

A number of field and laboratory studies have highlighted relationships between floc size, floc settling velocity, current shear stress and concentration, which have been summarized in the well known conceptual diagram by Dyer (1989). An increase in shear stress from rest initially enhances floc aggregation through an increase in particle collisions. As shear stress continues to increase, flocs reach a maximum size and break-up becomes the most important effect causing a reduction in floc size. This behaviour is also modulated by sediment concentration because of the increase in inter-particle collisions and also increases the probability of aggregation. The diagram by Dyer has been confirmed by a number of experiments (van Leussen, 1994; Manning and Dyer, 1999; Verney et al., 2011) and field observations (Fettweis et al., 2006; Braithwaite et al., 2012). However, this conceptual diagram only provides a simplified and partial understanding of the processes involved in flocculation. Indeed, in natural environments, flocculation is also impacted by a range of additional factors, such as hysteresis due to different time scales of aggregation and break-up (Verney et al., 2011), spatial variability (van Leussen, 1999; Fugate and Friedrichs, 2003), physico-chemical and biological effects van Leussen (1999), and sediment provenance (Jago and Jones, 1998; Bass et al., 2002; Fettweis et al., 2012).

Floc behaviour has been included in models via floc size and settling rate relationships of varying complexity (e.g., Winterwerp, 2002; Maerz et al.,

2011; Maggi, 2007). Validation of such models relies on long-term measurements of floc size, which remain scarce, and of settling velocities, which are difficult to measure *in situ*. In contrast to measurements based on settling columns which can disrupt the flocs and only work for low concentrations (free falling flocs), reliable floc sizes can be measured *in situ* using video images (Mikkelsen et al., 2006; Graham and Nimmo-Smith, 2010; Reynolds et al., 2010) and light diffraction techniques (Agrawal and Pottsmith, 2000; Reynolds et al., 2010; Davies et al., 2012). Formulations can then be used to obtain settling rates, such as the widely applied formula by Winterwerp (1998) which uses the floc diameter and fractal theory. Even though using fractal theory introduces complexity via an additional unknown factor (e.g., Camenen, 2009), there is, to date, no other method to deal with the floc complex structures.

Nevertheless, proposed formulations are still not capable of reproducing the wide scattering of the relationship between floc size and settling velocity. This is clearly observed in the compilations of different studies by Khelifa and Hill (2006) and Strom and Keyvani (2011) where plots of floc size against settling velocity show high data dispersion and low correlation coefficient values. This scattering seems to be strongly related to hydrodynamic conditions at temporal scales from intra-tidal to spring-neap cycles in addition to the factors mentioned previously. Indeed, flocculation is related to energy conditions from different hydrodynamic regimes as strong currents typically favour floc fragmentation while weak currents enhance floc aggregation. This behaviour is affected by kinetic energy differences between spring and neap tides, asymmetries during flood and ebb tidal phases, and sediment consoli-

dation during neap tides (e.g. Mehta, 1988; Sanford and Maa, 2001; Dankers and Winterwerp, 2007).

In addition, the impact of the combination of both currents and waves on the flocculation process is still not well known. Waves alone can cause seabed erosion and liquefaction which may have effects on the water column floc concentration. Bed shear stress also increases with the presence of both currents and waves (Soulsby, 1993) leading to changes in floc concentrations. We therefore still require a better understanding of the relationship between particle behaviour and turbulence under different hydrodynamic (waves and currents) conditions, in order to obtain better predictions of sediment transport in estuaries.

The present study seeks to improve our understanding of floc behaviour under the effect of different hydrodynamic conditions. We hypothesize that, in spite of the stochastic nature of flocs (Winterwerp et al., 2006; Maggi, 2008) and waves, scattering between turbulence and floc size can be reduced by using appropriate measures of turbulence under various hydrodynamic (i.e., combinations of waves and currents) regimes. Specifically, we propose the use of an effective kinetic energy instead of the widely used variables turbulence shear rate G, turbulent shear stress, or Kolmogorov microscale. To that end, we use *in situ* observations of floc size obtained from a LISST (Lasser In Situ Scattering and Transmisometry) and turbulence properties computed from high-frequency acoustic current meter data. Our case study enabled a comparison between three distinct hydrodynamic regimes: weak currents in absence of waves, combined effect of waves and currents, and dominant wave forcing. The observations are also split depending on tidal

phase (flood versus ebb), which is found to have a significant impact on the scattering between turbulence and floc size.

We describe the case study location in the next section and the observational methods in section 3. Results are presented in section 4, their interpretation and discussion in section 5. Finally the main findings are summarised in the conclusion.

2. Study area

Observations for this study were carried out in the Welsh Channel, one of the two channels connecting the Dee Estuary to the Liverpool Bay in the United Kingdom (Fig. 1). The Dee is a funnel shaped coastal plain estuary with a channel that bifurcates into the Welsh and Hilbre channels before entering Liverpool Bay (Fig. 1c). Most of the inner estuary remains very shallow with only the central channel at a depth of about 5 m below mean sea level. Depth then increases from the inner estuary towards the channels to 22 and 24 m for Hilbre and Welsh respectively. The channels finish with depths diminishing to less than 5 m depth in the outer part of the estuary.

The Dee is tidally dominated with a tidal range of about 10 m during spring tides and currents of more than 1 $m \cdot s^{-1}$ on the surface and nearly 0.5 $m \cdot s^{-1}$ near the seabed (Bolaños et al., 2013). Tides are significantly distorted due to the shallow nature of the estuary and tidal asymmetry results in flood dominance on sandy and muddy shallow areas, and weaker ebb dominance in the channels (Moore et al., 2009). In spite of the low river discharge, baroclinic behaviour remains important in the estuary, with stratification, tidal straining, wind and friction all having a role in the hydrodynamics of

both channels (Bolaños et al., 2013). Nevertheless, the residual spring tide is more important for the circulation of the Welsh Channel, while baroclinicity is more important for the circulation of the Hilbre Channel (Brown et al., 2014).

Suspended sediment concentrations increase from the Liverpool Bay to the inner part of the Dee estuary where muddy bed sediments prevail. Observations of suspended sediment concentration to the northwest of the estuary entrance, still in the Liverpool Bay, were of about 24 $mg{\cdot}l^{-1}$ in winter and 5 $mg{\cdot}l^{-1}$ in summer with size of about 100 μm for both suspended sediments at the surface and near the bottom (Krivtsov et al., 2008). At the entrance of the estuary, in the Hilbre Channel, Amoudry et al. (2014) reported maximum suspended sediment concentration of 500 $mg{\cdot}l^{-1}$ and Bolaños and Souza (2010) found dominance of fine flocs of about 70 μm in both channels. Inside the estuary, early measurements from bed samples by Turner et al. (1994) showed that the sediment fraction below 63 μm was present in percentages between 23% and 62%.

Because of the tidal dominance, SPM concentrations in the Dee Estuary are controlled by a combination of tidal advection and resuspension (Bolaños et al., 2009). The levels of accretion in the estuary indicate the Dee is a depository of sediments (Moore et al., 2009) with the sediment identified to mostly be of marine origin (Turner et al., 1994) which is in agreement with observations and modelling results that show bottom currents and sediment transport from the Liverpool Bay to the estuary entrance (e.g. Halliwell, 1973; Simpson and Sharples, 1991; Polton et al., 2011; Souza and Lane, 2013). However, according to Holden et al. (2011), it is possible that sediments

from the estuary contribute to the accretion of the Sefton coast to the north of the Dee. In addition, results by Moore et al. (2009) show a decrease in accretion rates which means the estuary is nearly in geomorphological equilibrium. The sediment transport in the estuary is not well known and is further complicated because of the presence of fine sediments leading to cohesive behaviour.

The dynamics of suspended sediments in the Dee estuary seems to mostly depend on turbulence, spatial distribution and biological factors. Classical links between turbulent properties and flocs in the Dee Estuary following which aggregation occurs during periods of weak turbulence (slack water at low and high tide) and break-up during periods of intense turbulence (maximum flood or ebb current) have been reported (e.g., Thurston, 2009; Ramírez-Mendoza et al., 2014) and included in numerical models (Ramírez-Mendoza et al., 2014). Amoudry et al. (2014) highlighted the importance of horizontal gradients in suspended sediment, themselves due to gradients in turbulence and bed sediment distribution, toward reproducing observed SPM behaviour in the Hilbre Channel.

3. Methodology

3.1. Observations

Observations for the present investigation were taken using a LISST (Laser In-Situ Scattering and Transmissometry) and an ADV (Acoustic Doppler Velocimeter) deployed in a tripod in the Welsh channel from 12 February to 8 March in 2008 at 1.5 and 0.3 metres above bottom, respectively. Details of the mooring and deployment can be found in Bolaños and Souza (2010).

198 The LISST uses laser diffraction techniques to measure floc sizes between
199 2.5-500 μm and their corresponding volume concentrations (Agrawal and
200 Pottsmith, 2000). For this study, the LISST recorded one sample every 40
201 seconds during a 20-minute period every hour. Data were then averaged to
202 obtain hourly measurements. The median floc size (D_{50}) was obtained from
203 the entire distribution as a single representative value of the floc size. Wa-
204 ter samples during days 12-13 February 2008 were taken each hour from a
205 CTD rosette for filtration on pre-weighted 0.4 μm mesh size filters. Filters
206 were weighted again to obtain mass concentration from the weight difference
207 before and after filtration and from water sample volume. A linear relation-
208 ship between these mass concentrations and corresponding LISST volume
209 concentrations enabled to find a calibration formulation to convert the entire
210 LISST recordings to mass concentrations (Ramírez-Mendoza et al., 2014).

211 The ADV employs the Doppler effect due to suspended particles to cal-
212 culate the flow velocity (SonTek, 2002). The instrument recorded current ve-
213 locity and pressure at 16 Hz during 20-minutes each hour at the same times
214 as the LISST allowing simultaneous measurements of both instruments. The
215 noise in ADV data was removed using a despiking algorithm based on a
216 three dimensional phase space method by Mori et al. (2007) which is based
217 on the method by Goring and Nikora (2002). We apply time-averaging of
218 the 20 minute sampling period in order to obtain hourly values of turbu-
219 lence statistics. Note that in the present investigation we are assuming a
220 logarithmic velocity profile and both instruments LISST and ADV are in the
221 approximately constant stress layer (Tennekes and Lumley, 1972).

3.2. Hydrodynamic features from ADV

Data measured by ADV are commonly used to extract information on near-bed turbulence following Reynolds decomposition of the velocity components. In the present study, we use the following decomposition to define velocity fluctuations:

$$u' = U - \overline{u} \qquad v' = V - \overline{v} \qquad w' = W - \overline{w} \tag{1}$$

where U, V, W are the three components of the instantaneous velocity, and $\overline{u}$, $\overline{v}$, $\overline{w}$ the three components of the mean (time-averaged) velocity. Shear stresses are then obtained using the covariances between fluctuations:

$$\tau_{cov} = \rho\sqrt{\overline{u'w'}^2 + \overline{v'w'}^2} \tag{2}$$

where ρ is water density. Shear stresses using equations 1 and 2 were obtained for the entire observation set from the ADV (with 20 minutes averaging). The energy from fluctuations in equation 1 is given by:

$$K = \frac{1}{2}(\overline{u'^2} + \overline{v'^2} + \overline{w'^2}) \tag{3}$$

which we refer to as effective kinetic energy. It is critical to note here that both the covariance stress τ_{cov} and the effective kinetic energy K include fluctuations that arise from both waves and turbulence. Many studies involving both turbulence and waves in coastal environments decompose into a wave contribution and a turbulence contribution instead (e.g. Trowbridge, 1998; Bricker and Monismith, 2007; Feddersen, 2012). Even though the overlap in the spatio-temporal scales affected by waves and turbulence, as well as potential wave-turbulence interactions, complicate such decomposition, several methods exist (e.g. Trowbridge, 1998; Bricker and Monismith, 2007).

However, in our case we focus on the effect of the fluctuations of fluid motion on sediment flocs. From the point of view of the floc (particle) mechanics, all fluid fluctuations act as an external force on the flocs, irrespective of their provenance whether wave-induced or turbulence-induced. It is therefore important here to use quantities that measure the full combined effect of all (wave and turbulence) fluctuations, as the covariance stress and the effective kinetic energy respectively defined in equations 2 and 3.

An analysis was made to the entire dataset in order to compare the individual effect of shear stress from currents and waves on sediment dynamics. Provided that wave characteristics are known, shear stress from waves and currents can be obtained following the spectral wave-current model of Madsen (1994). Wave height (H_s) and wave direction were obtained with the PUV method. This method calculates surface spectra $S_{\eta p}$ and $S_{\eta u}$ using pressure and velocity spectra S_p and S_u:

$$S_{\eta p} = \left(\frac{\cosh\, kh}{\cosh\, k(h+z)} \right)^2 \frac{S_p}{\rho_w^2 g^2} \tag{4}$$

$$S_{\eta u} = \left(\frac{\sinh\, kh}{\cosh\, k(h+z)} \right)^2 \frac{S_u}{\omega^2} \tag{5}$$

where k is wave number, h is mean water level relative to the seabed, z is vertical distance relative to the mean water level, ω is wave angular frequency (defined as 2πf, where f is frequency in cycles per second), ρ_w is water density and g is gravity. The value of k is calculated using the iterative Newton-Raphson method given by Wiberg and Sherwood (2008) in the wave dispersion relation:

$$\omega = \sqrt{gk \tanh kh} + kU_m \cos\alpha \tag{6}$$

where the second term on the right hand side is a modification to account for the presence of a mean current $U_m(=\sqrt{\overline{u}^2 + \overline{v}^2})$ with an angle α with the waves (Bolaños and Souza, 2010). The wave direction D_w is obtained using:

$$D_w = \arctan 2(S_{pu}, S_{pv}) \tag{7}$$

where $\arctan 2$ is fourth quadrant arctangent of the real parts of the cross-spectra between pressure-east velocity component (S_{pu}) and pressure-north velocity component (S_{pv}). Spectral energy integration was used to calculate the zeroth moment M_o and obtain the significant wave height (H_s) as:

$$H_s = 4\sqrt{M_o} \tag{8}$$

The peak period (T_p) is taken as the period with highest energy in the wave spectra. Wave orbital velocities can be obtained following the linear approach:

$$U_o = \frac{a_w \omega}{\sinh kh} \tag{9}$$

where a_w is wave amplitude ($H_s/2$). Madsen (1994) assumes simple periodic plane waves and proposes an iterative method to calculate friction velocities where the concept of wave friction factor is used. Thus:

$$\tau_w = \rho u_{*w}^2 \tag{10}$$

$$\tau_c = \rho u_{*c}^2 \tag{11}$$

$$\tau_{cw} = \rho u_{*cw}^2 \tag{12}$$

where τ is shear stress, ρ is fluid density, the $*$ symbol denotes friction velocity, subscripts w, c, cw are for waves, currents and combined waves and currents, respectively.

Dissipation of turbulent kinetic energy ϵ is estimated following the inertial dissipation method. This method assumes that radian wavenumbers k_r at which turbulence is produced are well separated from radian wavenumbers at which turbulent kinetic energy is dissipated by viscosity and this range is called the inertial range, where the flux of energy from high to low k_r must be equal to the dissipation range if no sources or sinks of turbulent kinetic energy are present (Huntley, 1988; Souza et al., 2011). Following Tennekes and Lumley (1972) and Voulgaris and Trowbridge (1998), the turbulent spectrum of the horizontal velocity component $E_u(k_r)$ is:

$$E_u(k_r) = \frac{9}{55}\alpha\epsilon^{2/3}{k_r}^{-5/3} \tag{13}$$

and the turbulent spectrum for the vertical velocity used in this study E_w is obtained as:

$$E_w(k_r) = \frac{4}{3}E_u(k_r) \tag{14}$$

where α=1.5 is the Kolmogorov constant. The spectra obtained from current velocities needs to be expressed as radian wavenumber k_r where the Taylor hypothesis or also called frozen turbulence concept is applied. Surface gravity waves could coincide with part of the inertial subrange. However, for this study, there was no overlap between waves and the turbulent inertial subrange. Once ϵ is known, the Kolmogorov microscale of turbulence (λ) and the turbulent shear parameter (G) were obtained following:

$$\lambda = \left(\frac{\nu^3}{\epsilon}\right)^{1/4} \tag{15}$$

$$G = \left(\frac{\epsilon}{\nu}\right)^{1/2} \tag{16}$$

where ν is kinematic viscosity.

4. Results

The analysis of the observations was divided in three regimes each five days long (Figs. 2 and 3). The first part occurs during neap tides (15 February to 20 February), wave heights are very small (<0.1 m), and the bottom current speed reaches up to 0.28 $m \cdot s^{-1}$. The ratio of current shear stress over wave shear stress, τ_c/τ_w, is the largest of the entire study with SPM concentration below 50 $mg \cdot l^{-1}$, and this part is therefore considered as a **"current-dominant"** regime. The second part occurs during spring tides (21 February to 26 February), bottom current speed reaches up to 0.5 $m \cdot s^{-1}$, and wave heights of 0.5 to 1.4 m are observed. The τ_c/τ_w ratio is significantly lower than during the previous regime, and this second part is defined as a combined **"currents-waves"** regime. During this regime was obtained the highest SPM concentration with 350 $mg \cdot l^{-1}$. The third and last part occurs again during neap tides (28 February to 05 March), bottom current speed is lower than for the first regime (less than 0.2 $m \cdot s^{-1}$), and waves are the highest of the entire record with nearly 2 m height reached. The τ_c/τ_w ratio is the lowest of the study, and this regime is considered to be **"wave-dominant"**. Maxima of SPM concentration coincided with the highest wave heights and concentration of about 150 $mg \cdot l^{-1}$.

4.1. The floc size spectrum

Floc sizes measured by the LISST are shown for the three regimes in figure 4 with volume concentrations converted to mass concentrations. Since observations were taken during winter we assume the effect of organic material was minimal as has been found by some authors (e.g. Le Hir et al., 2007;

Fettweis et al., 2014) and in the Dee estuary by Todd (2014). An important feature of the floc size observations is the presence of one concentration peak at any time. This means the floc distribution is unimodal and the use of D_{50} is a reasonable approximation. During the first regime (Fig. 4a), high concentrations of small flocs coincided with flood and ebb phases while the high concentrations of large flocs happened with depth maxima and minima (close to slack water in the Dee). Concentrations diminished through the neap tide period but increased with tides at the end of the record. The "currents-waves" regime (Fig. 4b) presented the highest concentrations of both small and large flocs. Floc behaviour was similar as in the "current-dominant" case but amplified due to the hydrodynamic conditions and flocs reached the smallest size during this period. In the "wave-dominant" regime, concentrations were generally similar to the "current dominant" regime but lower than the "currents-waves" regime, except for two maxima on 1st March, and the relationship between floc size and tidal forcing is not as regular as in previous cases.

As expected, the behaviour of the flocs seems to be the result of turbulence-induced flocculation. Even though mass SPM concentration increases during resuspension events, there is no evidence of floc aggregation may be due to low SPM concentrations. Overall, the measured range of small and large flocs were $\sim$50-100μm and $\sim$300-350μm, respectively. During strong currents on flood and ebb, flocs in suspension are subjected to strong shear stresses and inter-particle collisions which result in break-up of large flocs and the measurement of high concentrations of small flocs. When shear stresses diminish around slack water, small flocs in suspension aggregate to form large flocs

and lead to diminish the concentration of small flocs and increase concentration of large flocs. Overall, from neap to spring tides there is an increase of shear stresses resulting in higher floc resuspension and break-up leading to the smallest floc sizes in flood and ebb of spring tides. The higher concentration of small flocs leads to aggregation enhancement and bigger flocs during slack waters. The relative concentrations of small and large flocs are therefore determined by the turbulence magnitude, which is influenced by the presence of currents and waves. The mild conditions during the first regime were overwhelmed by the combination of both waves and currents in the second regime and the waves had the most important effect during the third regime with concentration maxima coinciding with the highest wave height.

4.2. Separated effect of currents and waves on flocculation

Time series of shear stress from waves τ_w and currents τ_c are presented in figure 5 along with median floc size D_{50} for the three hydrodynamic regimes. The "current-dominant" regime (Fig 5a) confirms that shear stress from waves was negligible in comparison with stress from currents. This regime showed an increase in shear stress magnitude from about 0.10 Pa to 0.35 Pa towards the spring tide which means more energetic conditions and thus floc break-up. This is consistent with the general trend for the floc size following which the intra-tidal minimum floc size diminished from 70 μm to 60 μm and the intra-tidal maximum floc size diminished from 240 μm to 160 μm, both over the duration of this regime. There was a clear quarter-diurnal variability for the shear stress with flood-ebb asymmetry showing higher values during ebb than during flood. This asymmetry resulted in stronger floc disaggrega-

tion during the ebbs, and ebb flocs smaller than flood flocs. Minimum values of shear stress also presented differences with effects on floc sizes. Shear stress minima after ebb phase had considerably lower values than after flood and this allowed floc growth resulting in smallest flocs during slack waters after ebb.

For the "currents-waves" regime (Fig 5b), shear stress from waves had the same order of magnitude as shear stress from currents, in particular during the first two days. Both stresses reached in excess of 0.75 Pa on 22 February. Wave stress was tidally modulated and in phase with current stress with the same quarter-diurnal variability persistent throughout the entire period. This tidal modulation of waves has already been reported for the Dee estuary by Bolaños et al. (2014). From the processes causing a wave tidal modulation mentioned by Davidson et al. (2009), the current-wave interaction itself is maybe the main factor happening in the study site. The combination of stress from waves and currents resulted in the smallest flocs (50 μm) of the three regimes, while the largest flocs barely reached 150 μm, in particular during the first two days when waves were the largest for this regime. During the last two days, wave stress diminished and floc size behaviour became qualitatively identical to that of the "current-dominant" regime although the size of the small flocs remained in 50 μm due to spring tide hydrodynamic forcing. The resulting floc size variability was the highest of the three regimes, with a range of 50-225 μm. The quarter-diurnal behaviour was similar to that of the previous regime with weaker shear stress during flood than ebb. However, D_{50} minima were of similar magnitude ($\sim$ 50 μm) although slightly diminished to the end of record when shear stress from waves was half the

magnitude of the stress of currents. During slack waters in this regime large flocs were present as in the "current-dominant" regime, with the largest flocs after ebb phase and an important difference with floc size after flood that reached 100 μm on 23 February.

The "wave-dominant" regime is shown in figure 5c where shear stress from waves reached more than 2 Pa, and those from currents remained about 0.5 Pa as in previous regimes. In this regime, wave shear stresses almost lost the neap-spring tidal modulation and also the quarter-diurnal variability found in the combined regime. The highest wave shear stresses were present during three consecutive days (1-3 March). These maxima coincided with the smallest median floc sizes of about 60 μm in this regime. These periods were followed by calm conditions and an increase in D_{50} values of more than 180 μm. Floc behaviour during this regime was therefore the response only to wave conditions and also the highest shear stresses were present during this regime. Nevertheless, these not resulted in the smallest median floc sizes and instead showed the lowest D_{50} variability of the three regimes which may represent an equilibrium between floc break-up and aggregation around 60 μm.

In summary: (i) the "current-dominant" regime had the highest floc size variability with clear floc aggregation and break-up, (ii) with the "currents-waves" combined effect floc break-up became dominant and aggregation diminished, and (iii) when shear stress from waves is more important seems to be a balance of aggregation and break-up processes. Therefore, the effect of generated turbulence from currents and waves on the flocculation process seemed to affect at different magnitudes and maybe in different ways.

However, the specific behaviour of the flocs in response to the turbulence conditions from the three different regimes is still unknown. In addition, D_{50} asymmetries between flood and ebb phases appeared to reflect effects of turbulence which depends on flow direction. The next section analyses the relationships of the median floc size and turbulent properties important for the flocculation process.

4.3. Flocculation controls

Relationships between median floc size and shear stress, effective kinetic energy and dissipation rate are shown in figure 6 for the entire dataset covering all three regimes. Shear stresses using the covariance (Eq. 2) and spectral (Eq. 12) methods are shown in figures 6a and 6b, respectively. Both shear stresses presented an inverse relationship with median floc size, although τ_{cov} had higher values and τ_{cw} presented a slightly different data distribution, with a small amount of data corresponding to large flocs and about $1{\times}10^{-2}$ Pa while small flocs presented a wider distribution.

The relationship between D_{50} and K also showed an inverse relationship in a clearly defined population (Fig. 6c). Dissipation (Fig. 6d) has been included because it is used to calculate shear rate G and the Kolmogorov microscale of turbulence λ. This showed two populations, one with similar inverse relationship as the other variables and a second population for dissipation approximately constant. From all the relationships, floc size with τ_{cov} and K had the simplest distributions since only one population of data can be distinguished. Furthermore, a lower scatter of points is obtained when relating D_{50} to K, which would result in a decrease in the uncertainty when a curve fitting is applied to the data (R^2 value using τ_{cov} is 0.48 while using

K is 0.58). Even though the variability of median floc size remains high for a given value of effective kinetic energy, this range of floc sizes is smaller than for any of the other variables τ_{cov}, τ_{cw} and ϵ. These results suggest that K may give better approximations if used to describe floc size changes. To further analyse this hypothesis, values of τ_{cov} and K were divided in hydrodynamic regimes and flood and ebb phases. In addition, to observe the effects of the dissipation rate on other variables, the same analysis is carried out for the Kolmogorov microscale and shear parameter.

4.4. Shear stress and effective kinetic energy

Observations relating D_{50} and τ_{cov} are shown in figure 7 in panels a, c, and e for "current-dominant", "currents-waves" and "wave-dominant" regimes, respectively, and flood and ebb phases. The range of τ_{cov} values is slightly different for each regime. As expected, highest τ_{cov} values were obtained during the "currents-waves" regime while the lowest during the "current-dominant" regime. In contrast, the "wave-dominant" case showed the lowest variability of shear stress. Floc sizes mainly differ in minimum values. The smallest flocs during the "current-dominant" and "wave-dominant" regimes were of about 60 μm diameter, while the smallest flocs in the "currents-waves" regime were about 40 μm according to the highest values of τ_{cov} for this case. The most important feature is that the relationship follows the same pattern during flood and ebb phases. These phases show only a shift but the distribution remains the same and the magnitude of the shift seems to be similar for the three regimes. Unlike the "current-dominant" regime, "currents-waves" and "wave-dominant" regimes present a wide scatter of data.

Figure 7 in panels b, d and f shows the relationship during the three regimes and flood and ebb tidal phases between K and D_{50}. All regimes showed the same behaviour, like in the case of τ_{cov}, an inverse relationship with differences in magnitudes and tidal phases. The "current-dominant" and "currents-waves" regimes were characterised by higher energy during ebb phases. This intratidal difference in effective kinetic energy magnitude means the shift previously found is also present in these two regimes for the energy variable although smaller than the shift for the τ_{cov} case. The difference between flood and ebb is almost undistinguishable during the "wave-dominant" regime (Fig. 7f).

Results of the relationships between median floc size, shear stress and effective kinetic energy demonstrate the possibility to describe the floc behaviour with simple formulations derived from the log-log plots of the variables. Moreover, better quantitative results should be obtained if flood and ebb tidal phases are also taken into account.

4.5. Turbulent shear parameter and Kolmogorov microscale

Another commonly used property to assess the turbulence effect on the flocculation process is the shear parameter G, shown in figure 8 (panels a, c and e), which is a measure of the turbulent shear rate in the flow and therefore strongly related to floc sizes. Despite the wide scatter of data, two populations can be distinguished in figures 8a and 8c. A large population during ebb phase with, as expected, an inverse relationship shows small flocs for high shear rate and increasing sizes with decreasing shear rate. A second small population appears almost in the middle of the aforementioned population during flood and is characterised by approximately constant G values.

However, a random behaviour is also noticeable when floc size increases above 100 μm. This is also present during the ebb phase in the "current-dominant" regime. The "wave-dominant" regime is characterised by a wide spread of data without any important difference between flood and ebb phases or different populations (Fig. 8e). Differences between the three regimes and flood and ebb tidal phases are present but there is no single relationship for all the cases.

The smallest eddies in the turbulent flow are represented by the Kolmogorov microscale λ, which is assumed to be a floc size threshold (e.g. Winterwerp and van Kesteren, 2004). Results for this study are shown in figure 8 panels b, d and f for the three regimes. Data show two clear different populations when flocs are smaller than 200 μm with a similar data scattering as for the shear rate G. One of these populations is further identified as occurring during flood for the "current-dominant" (Fig. 8b) and "currents-waves" (Fig. 8d) regimes with low variability of λ values. No clear behaviour was found for floc sizes larger than 200 μm in any tidal phase of the "current-dominant" regime while for the ebb phase in "currents-waves" regime a direct relationship was present for all floc sizes. A different case was shown for the "wave-dominant" regime when the differences between tidal phases were not as clear as in previous cases although a direct relationship is present with a wide data scattering (Fig. 8f).

5. Discussion

The "current dominant" regime is probably the simplest of the three regimes and the one where the flocculation response to turbulent conditions

is most evident. In general, the floc sizes are larger during neap tides than during spring tides as a result of weaker turbulent conditions (Fig. 5a). Low turbulence allows floc aggregation while break-up is not enough strong during neaps. These conditions change during spring tides and break-up becomes important. There is also interesting behaviour of the floc size variability at the semidiurnal frequency. Shear stress minima after ebb phase falls to nearly zero values coinciding with large flocs (see for example figure 5a at the end of day 15) while after flood stress is not as low and flocs are not as large as after ebb (see figure 5a on day 16 after the first grey bar). Large flocs at low water could be the result of aggregation of small flocs due to turbulent motions and either locally resuspended, or advected from upper parts of the estuary during the long ebb phase since advection of suspended sediments is an important process in the Dee Estuary under such calm neap tide conditions (Amoudry et al., 2014). Asymmetries in shear stress maxima coincide with asymmetries in floc size minima as a direct result of turbulence magnitude. For example, in figure 5a on the first half of day 17 the maxima stresses were $\sim$0.08 Pa for flood and $\sim$0.14 Pa for ebb with floc sizes of $\sim$100 μm and $\sim$90 μm, respectively (ellipses in fig. 5a).

The "currents-waves" regime is characterized by an enhancement of the conditions of the "current dominant" case, with higher concentrations of smaller and larger flocs for high and low energy conditions, respectively. The combined effect of currents and waves shear stresses first resuspends small flocs from the bed to upper parts of the water column, then resuspends large flocs which are subsequently disaggregated and thus measured as small flocs. Other possibility is that particles are firstly resuspended from the bottom,

then aggregate and formed flocs adjust to the present turbulent conditions. Since waves are tidally modulated (Bolaños et al., 2014), the decrease in shear stress from waves and currents is likely to occur at nearly the same time and enhances the aggregation of suspended flocs which are measured as large flocs in also high concentrations.

Shear stress during the "wave-dominant" regime was the highest of the entire record and therefore the highest erosion, resuspension and disaggregation were expected. However, concentrations are lower and flocs are not as small as during the "currents-waves" regime. It is possible that in the "currents-waves" case high concentrations are present at low levels while in the "wave-dominant" case with higher energy conditions suspended sediments could be dispersed over the entire water column and thus not recorded by measurements at a given level. Bartholomä et al. (2009) measured suspended sediments through the water column in higher concentrations during high waves conditions than during calm periods and modelling results by Stanev et al. (2006) also showed this behaviour. Even though the "currents-waves" is the regime with extreme floc sizes, a more important comparison is between the "current dominant" and "wave-dominant" regimes as these occurred during similar tidal conditions. Floc behaviour in response to tidal currents is almost completely overwhelmed by the presence of waves, which are only slightly affected by tidal modulation.

Floc size changes seem to be also related to their distribution in the water column. As mentioned before, the flocculation process is enhanced during the "currents-waves" regime. However, the "wave-dominant" regime is characterised by longer periods of sustained high shear stress. In these

conditions flocs at the seabed are taken into suspension and a possible "steady state" could be achieved near the bottom as described by Puls et al. (1988). According to the authors, a "steady state" may occur if flocs in higher parts of the water column, away from the bottom but far enough from the surface, are subjected to less turbulent conditions and therefore aggregate to bigger flocs which then fall to high energy lower parts where they disaggregate and are again raised to higher parts. This could explain the floc size low variability during the higher energy events of the "wave-dominant" regime. A second possible explanation is that a longer effect of shear stress causes the erosion of flocs in the process of consolidation on the sea bed but is not enough to break them and therefore remain slightly larger than the firstly resuspended weak flocs. There is also another possibility for the floc size low variability during this regime and is that flocs aggregate to a certain size and cannot continue growing because of the sustained agitation by both waves and turbulence. At the end of this regime the floc size range increase, 100-240 μm, and this is likely due to the flocs left in suspension by the effect of waves. The wave shear stress decrease during the last one and a half days allowing for the currents shear stress to be the dominant effect with the semidiurnal variability, but with a higher floc size range. A decrease in this range and similar behaviour to the "current dominant" regime are expected if no more waves are present.

5.1. D_{50} relationships with τ_{cov} and K

Data scattering for all hydrodynamic regimes and all tidal phases seems to be lower in the relationship of D_{50} with K than with τ_{cov} as shown in figure 7. This suggested the possibility to describe floc size changes using

simple equations of a power of the effective kinetic energy of the form: D_{50}= $A \cdot (K)^B$. Using this form, a test was carried out adjusting curves to the data distributions of figure 7. The resulting coefficients of determination R^2, are shown in table 5.1 in order to compare the use of K and τ_{cov} for the description of floc size, as well as how the regime and tidal separation improves their relationship. Except for the flood phase during the "current only" regime, the use of effective kinetic energy produces the best fits to the data according to R^2 values. Improvements from 2% ("current dominant"-ebb) to 26% ("wave-dominant"-ebb) and of 30% for the "wave-dominant" regime and both phases are reached using K. The minimum R^2 difference is obtained in the "current dominant" regime, it increases in the combined regime and is maximum in the "wave-dominant" regime, which emphasizes the important role of the waves in the process. Therefore, a better floc size predictor seems to be the effective kinetic energy instead of the widely used turbulent stress or turbulent shear rate (e.g. Winterwerp et al., 2006; Manning et al., 2010; Kombiadou and Krestenitis, 2012). This also seems to be particularly true in the presence of waves.

5.2. D_{50} relationships with G and λ

The relationships between floc size D_{50} and the turbulent shear parameter G follow the behaviour reported by different authors during ebb and part of the flood (e.g. Mietta et al., 2011; Verney et al., 2011; Wang et al., 2013), i.e. low shear rate corresponds to larger flocs and their size decrease as shear rate increase. The high scatter floc behaviour for the "current-dominant" regime at low G values has also been found in other studies (Winterwerp, 1998; Verney et al., 2011). The "currents-waves" regime during ebb has a clear

aggregation and disaggregation behaviour. Higher data scattering was found during the "wave-dominant" case on both flood and ebb phases. Turbulent shear rate seems to have the expected effect during ebb phases. Flocs in the present study were smaller than the Kolmogorov microscale which is in agreement with different studies (e.g. Braithwaite et al., 2012; Fettweis et al., 2006; Cross et al., 2013; Son and Hsu, 2011), larger flocs than λ have also been reported (e.g. Cross et al., 2013). In addition, flocs cannot reach the Kolmogorov microscale on either hydrodynamic regime or tidal phase. The specific behaviour of the Kolmogorov microscale is similar to the shear parameter, increase in λ coincides with increase in median floc size for ebb and part of the flood phases when flocs were higher than 200 μm.

The Kolmogorov microscale relationship with D_{90} floc size is shown in figure 9 for comparison with $\lambda - D_{50}$ relationship in figure 8. Overall, D_{90} values are about $150\mu m$ higher than D_{50} with similar time series behaviour (data not shown) as has also been found experimentally by Verney et al. (2011). The use of D_{90} led the floc sizes around the Kolmogorov microscale with good correlation for the ebb phase in all the regimes. However, slightly larger values in the case of the "current-dominant" regime can be seen and also some values were higher than the instrument upper limit. This is not as clear during the other two regimes. Flood phases still presented the same behaviour as for the D_{50} case.

The difference between flood and ebb behaviour of G and λ is related with asymmetries in turbulent dissipation. These asymmetries are shown in figure 10 with the expected semidiurnal variability. Overall, during ebb phase dissipation values were higher than during flood with differences of about one

order of magnitude. In particular, dissipation variability during flood phases is lower than during ebb. Extreme minima values are also observed at low slack waters mainly during the first two regimes which correspond with some of the randomly results at large floc sizes in figure 8a to 8d and occur when turbulence is maybe too low for the dissipation calculations be valid.

5.3. Flood and ebb tidal phases

The scatter of data still present when observations are divided into flood and ebb phases may be due to the hysteresis effect. This is one of the most important and scarcely mentioned features of the cohesive sediment behaviour and its effect can be seen in the relationship of a number of different variables: turbulent stresses, SPM concentration, current speed, Reynolds stresses, turbulent kinetic energy and median floc size (e.g. Dyer, 1986; Fettweis et al., 2012; Wang et al., 2013). It has been stated that this effect is due to a time lag in the response between different variables (e.g. Verney et al., 2011). The floc size behaviour during flood and ebb periods in the present study is similar to results in the Belgian coast presented by Fettweis et al. (2012). The authors showed periods of neap tides without the effect of waves with clear difference between the flood and ebb periods as in the "current only" and "currents-waves" regimes, while during storms the observations showed high scatter with a slight difference between tidal phases as in the "wave-dominant" case.

Figure 11 shows an example of the hysteresis effect during a tidal cycle of the present investigation. The flood phase starts at low energy conditions (red triangle). The floc size diminishes as the energy increases until the system reaches maximum energy and a minimum median floc size. When

the energy decreases, the floc size increases with values slightly greater until the phase finishes (red circle). The behaviour during the ebb phase (in blue) is similar in floc size changes but with a shift in the values of turbulent kinetic energy. This particular feature seems to add another variable to the flocculation process since the size of the flocs at the end of one phase is important for the beginning of the next phase, i.e., the effect of the turbulence will be different on flocs of slightly different sizes and also small changes in turbulence will have a different effect. In summary, the first characteristic of the behaviour of the floc size with respect to turbulent properties is their inverse relationship, the second feature is the shift between tidal phases and the third is the hysteresis phenomenon. The last two characteristics may explain part of the important scattering in the observations during the same tidal phase.

6. Conclusions

In the present investigation the response of the flocculation process due to turbulence from different hydrodynamic conditions and intra-tidal variability was investigated. To achieve this, field observations were used to characterise floc size behaviour in a hypertidal estuary. Three hydrodynamic regimes were defined based on the magnitude of the effect of currents and waves.

During the "currents-dominant" regime currents were the main forcing factor and typical floc aggregation and break-up was found with low and high energy conditions, respectively. The presence of waves in the "currents-waves" regime coincided with strong currents in spring tides enhancing the turbulence-induced flocculation process. Floc sizes during this second regime

presented the highest variability of the entire study. High shear stress led to the smallest flocs while low shear stress to a wide range of large flocs because of break-up and aggregation, respectively. During the "wave-dominant" regime waves were the most important forcing factor and shear stresses reached their highest values. However, flocculation was significantly diminished with floc sizes showing almost constant values coinciding with the highest waves. This could be due to floc distribution along the water column or a possible floc steady state.

The relationships of floc size and shear stress and effective kinetic energy, showed the commonly found inverse relationship and high data scattering. In the case of effective kinetic energy, the scattering was lower suggesting a better predictor of floc size. Data separation in hydrodynamic regimes and flood-ebb phases also reduced significantly the data scattering with the intra-tidal variability characterised by a shift while still showing the inverse relationship. The only exception was the "wave-dominant" regime. These results are confirmed when curve fittings were applied to these separated data resulting in improvements of the determination coefficients R^2 of up to 26%. Overall, determination coefficients of the separated distributions were better for effective kinetic energy than for shear stress.

The relationship between floc size and turbulent shear rate showed the expected inverse relationship only during ebb phases while during flood changes in floc sizes happened with low variability of G values. Median floc size was lower than the Kolmogorov microscale of turbulence which is anticipated because of the winter season. During flood the Kolmogorov microscale presented low variability. The low variability of both G and λ during flood was

related to current tidal asymmetries. These tidal differences seem to be enhanced when dissipation values are calculated (Eq. 14) and in turn used to calculate the Kolmogorov microscale of turbulence and turbulent shear rate (Eqs. 15 and 16).

Results of this study showed hydrodynamic conditions are important for the floc size behaviour and part of the wide data scattering is explained by flood and ebb tidal phases with the hysteresis effect also playing an important role. Taking into account these features may lead to better results when proposing formulations to describe the flocculation process. In particular, the use of an effective kinetic energy instead of shear stresses in numerical models could result in improved predictions of flocculation when both currents and waves are present.

Acknowledgements

We want to acknowledge the organizations of the United Kingdom and México which provided the funding and oportunity for this investigation to be carried out: NERC (National Environmental Research Council via the iCOASST project, grant NE/J005444/1), NOC (National Oceanography Centre) and CONACyT (Consejo Nacional de Ciencia y Tecnología throught the PhD Scholarship ID 212026), CICESE (Centro de Investigación Científica y de Educación Superior de Ensenada). We also want to thank Dr. Romaric Verney for his important comments to improve the study presented in this manuscript.

References

Agrawal, Y., Pottsmith, H., 2000. Instruments for particle size and settling velocity observations in sediment transport. Marine Geology 168, 89–114.

Amoudry, L. O., Ramírez-Mendoza, R., Souza, A. J., Brown, J. M., 2014. Modelling-based assessment of suspended sediment dynamics in a hyper-tidal estuarine channel. Ocean Dynamics 64, 707–722, dOI 10.1007/s10236-014-0695-8.

Bartholomä, A., Kubicki, A., Badewien, T. H., Flemming, B. W., 2009. Suspended sediment transport in the German Wadden Sea—seasonal variations and extreme events. Ocean Dynamics 59, 213–225.

Bass, S., Aldridge, J., McCave, I., Vincent, C., 2002. Phase relationships between fine sediment suspensions and tidal currents in coastal seas. Journal of Geophysical Research 107 (C10), 10–1–10–14, dOI:10.1029/2001JC001269.

Bolaños, R., Brown, J. M., Amoudry, L. O., Souza, A. J., 2013. Tidal, Riverine and Wind Influences on the Circulation of a Macrotidal Estuary. Journal of Physical Oceanography 43, 29–50, dOI: 10.1175/JPO-D-11-0156.1.

Bolaños, R., Brown, J. M., Souza, A. J., 2014. Wave-current interactions in a tide dominated estuary. Continental Shelf Research 87, 109–123, dOI: 10.1016/j.csr.2014.05.009.

Bolaños, R., Moate, B., Souza, A. J., 2009. Measuring suspended sediment and its wave and turbulence forcing in the dee estuary. In: Mizuguchi, M.,

Sato, S. (Eds.), Coastal Dynamics 2009: Impacts of human activities on dynamic coastal processes, Japan. World Scientific. Vol. 43. p. 12, paper 119.

Bolaños, R., Souza, A. J., 2010. Measuring hydrodynamics and sediment transport processes in the Dee Estuary. Earth System Science Data 2, 157–165.

Braithwaite, K., Bowers, D., Nimmo-Smith, W., Graham, G., 2012. Controls on floc growth in an energetic tidal channel. Journal of Geophysical Research 117, 1–12, doi:10.1029/2011JC007094.

Bricker, J., Monismith, S., 2007. Spectral wave-turbulence decomposition. Journal of Athmospheric and Ocean Technology 24 (8), 1479–1487, doi:10.1175/JTECH2066.1.

Brown, J. M., Bolaños, R., Souza, A. J., 2014. Process contribution to the time-varying residual circulation in tidally dominated estuarine environments. Estuaries and Coasts 37, 1041–1057, dOI 10.1007/s12237-013-9745-6.

Camenen, B., 2009. Discussion of Uncertainty of excess density and settling velocity of mud derived from in situ measurements by M. Fettweis. Estuarine Coastal & Shelf Science 78(2), June 2008. doi: 10.1016/j.ecss.2008.01.007. Estuarine, Coastal and Shelf Science 83, 111–112, doi:10.1016/j.ecss.2008.08.013.

Cross, J., Nimmo-Smith, W., Torres, R., Hosegood, P., 2013. Biological controls on resuspension and the relationship between particle size and the

790 kolmogorov length scale in a shallow coastal sea. Marine Geology 343,
791 29–38.

792 Dankers, P., Winterwerp, J., 2007. Hindered settling of mud flocs:
793 Theory and validation. Continental Shelf Research 27, 1893–1907,
794 doi:10.1016/j.csr.2007.03.005.

795 Davidson, M., O'Hare, T., George, K., 2009. Tidal modulation of incident
796 wave heights: Fact or Fiction? Reef Journal 1 (1), 16–32.

797 Davies, E., Nimmo-Smith, W., Agrawal, Y., Souza, A., 2012. Lisst
798 100 response to large particles. Marine Geology 307-310, 117–122,
799 doi:10.1016/j.margeo.2012.03.006.

800 Dyer, K. R., 1986. Coastal and Estuarine Sediment Dynamics. John Wiley
801 & Sons, pp 342.

802 Dyer, K. R., 1989. Sediment processes in estuaries: future research require-
803 ments. Journal of Geophysical Research 94 (C10), 14327–14339.

804 Feddersen, F., 2012. Observations of the surf-zone turbulent dissipation rate.
805 Journal of Physical Oceanography 42 (3), 386–399.

806 Fettweis, M., Baeye, M., Lee, B., Chen, P., Yu, J., 2012. Hydro-
807 meteorological influences and multimodal suspended particle size distri-
808 butions in the belgian nearshore area (southern north sea). Geo-Marine
809 letters 32, 123–137, dOI 10.1007/s00367-011-0266-7.

810 Fettweis, M., Baeye, M., Van der Zande, D., Van den Eynde, D., Lee, B.,

2014. Seasonality of floc strength in the southern north sea. Journal of Geophysical Research 119, 1911–1926, dOI 10.1002/2013JC009750.

Fettweis, M., Francken, F., Pison, V., Van den Eynde, D., 2006. Suspended particulate mater dynamics and aggregate sizes in a high turbitidy area. Marine Geology 235, 63–74.

Fugate, D., Friedrichs, C., 2003. Controls on suspended aggregate size in partially mixed estuaries. Estuarine, Coastal and Shelf Science 58, 389–404.

Goring, D., Nikora, V., 2002. Despiking acoustic doppler velocimeter data. Journal of Hydraulic Engineering 128 (1), 117–126, 10.1061/(ASCE)0733-9429(2002)128:1(117).

Graham, G. W., Nimmo-Smith, A. M., 2010. The application of holography to the analysis of size and settling velocity of suspended cohesive sediments. Limnology and Oceanography: Methods 8, 1–15.

Halliwell, A., 1973. Residual drift near the sea bed in Liverpool Bay: an observational study. Geophysical Journal of the Royal Astronomical Society 32, 439–458.

Holden, V., Worsley, A., Booth, C., Lymbery, G., 2011. Characterisation and sediment-sourde linkages of intertidal sediment of the UK's north Sefton coast using magnetic and textural properties: findings and limitations. Ocean Dynamics 61 (12), 2157–2179.

Huntley, D., 1988. A modified inertial dissipation method for estimating seabed stresses at low Reynolds numbers, with application to wave/current

boundary layer measurements. Journal of Physical Oceanography 18, 339–346.

Jago, C. F., Jones, S. E., 1998. Observation and modelling of the dynamics of benthic fluff resuspended from a sandy bed in the Southern North Sea. Continental Shelf Research 18 (11), 1255–1282.

Khelifa, A., Hill, P. S., 2006. Models for effective density and settling velocity of flocs. Journal of Hydraulic Research 44 (3), 390–401.

Kombiadou, K., Krestenitis, N. Y., 2012. Fine sediment transport model for river influenced microtidal shelf seas with application to the thermaikos gulf. Continental Shelf Research 36, 41–62.

Krivtsov, V., Howarth, M. J., Jones, S. E., Souza, A. J., Jago, C. F., 2008. Monitoring and modelling of the irish sea and liverpool bay: An overview and spm case study. Ecological Modelling 212, 37–52.

Le Hir, P., Monbet, Y., Orbain, F., 2007. Sediment erodability in sediment transport modelling: Can we account for biota effects? Continental Shelf Research 27, 1116–1142, doi:10.1016/j.csr.2005.11.016.

Madsen, O., 1994. Spectral wave-current bottom boundary layer flows. In: Edge, B. (Ed.), Proceedings of the 24th International Conference on Coastal Engineering. ASCE, pp. 384–398, Kobe, Japan.

Maerz, J., Verney, R., Wirtz, K., Feudel, U., 2011. Modeling flocculation processes: Intercomparison of a size class-based model and a distribution-based model. Continental Shelf Research 31, S84–S93, doi:10.1016/j.csr.2010.05.011.

857 Maggi, F., 2007. Variable fractal dimension: A major control for floc struc-
858 ture and flocculation kinematics of suspended cohesive sediment. Journal
859 of Geophysical Research 112 (C07012), 1–12.

860 Maggi, F., 2008. Stochastic flocculation of cohesive sediment: Analysis of
861 floc mobility within the floc size spectrum. Water Resources Research
862 44 (WO1433), doi:10.1029/2007WR006109.

863 Manning, A., Baugh, J., Spearman, J., Whitehouse, R., 2010. Flocculation
864 settling characteristics of mud: sand mixtures. Ocean Dynamics 60, 237–
865 253.

866 Manning, A., Dyer, K., 1999. A laboratory examination of floc characteristics
867 with regard to turbulent shearing. Marine Geology 160, 147–170.

868 Mehta, A., 1988. Laboratory studies on cohesive deposition and erosion. In:
869 Dronkers, J., van Leussen, W. (Eds.), Physical Processes in Estuaries.
870 Springer-Verlag, p. 560.

871 Mietta, F., Chassagne, C., Verney, R., Winterwerp, J., 2011. On the behavior
872 of mud floc size distribution: model calibration and model behavior. Ocean
873 Dynamics 61, 257–271, dOI 10.1007/s10236-010-0330-2.

874 Mikkelsen, O. A., Hill, P., Milligan, T., 2006. Single-grain, mi-
875 crofloc and macrofloc volume variations observed with a lisst-100
876 and a digital floc camera. Journal of Sea Research 55, 87–102,
877 doi:10.1016/j.seares.2005.09.003.

878 Moore, R., Wolf, J., Souza, A., Flint, S., 2009. Morphological evolution of

879 the dee estuary, eastern irish sea, uk: A tidal asymmetry approach. Geo-
880 morphology 103, 588–596, doi:10.1016/j.geomorph.2008.08.003.

881 Mori, N., Suzuki, T., Kakuno, S., 2007. Noise of acoustic doppler velocime-
882 ter data in bubbly flows. Journal of Engineering Mechanics 133, 122–125,
883 doi:10.1061/(ASCE)0733-9399(2007)133:1(122).

884 Polton, J., Palmer, M., Howarth, M., 2011. Physical and dynamical oceanog-
885 raphy of Liverpool Bay. Ocean Dynamics 61, 1421–1439.

886 Puls, W., Kuehl, H., Heymann, K., 1988. Settling velocity of mud flocs:
887 results of field measurements in the Elbe and the Weser Estuary. In:
888 Dronkers, J., van Leussen, W. (Eds.), Physical Processes in Estuaries.
889 Springer-Verlag, p. 560.

890 Ramírez-Mendoza, R., Souza, A., Amoudry, L., 2014. Modeling flocculation
891 in a hypertidal estuary. Ocean Dynamics 64, 301–313, dOI 10.1007/s10236-
892 013-0675-4.

893 Reynolds, R. A., Stramski, D., Wright, V. M., Woźniak, 2010. Measurements
894 and characterization of particle size distribution in coastal waters. Journal
895 of Geophysical Research 115, 1–19.

896 Sanford, L., Maa, J.-Y., 2001. A unified erosion formulation for fine sedi-
897 ments. Marine Geology 179 (1-2), 9–23.

898 Simpson, J., Sharples, H., 1991. Coastal and Estuarine Studies. Dynamics
899 and Exchange in Estuaries and the Coastal Zone. American Geophysical
900 Union, Ch. 6. Dynamically-active models in the prediction of estuarine
901 stratification, pp. 101–113.

902 Son, M., Hsu, T., 2011. The effects of flocculation and bed erodibility on
903 modeling cohesive sediment resuspension. Journal of Geophysical Research
904 116 (C03021), 1–18.

905 SonTek, 2002. SonTek ADVField Acoustic doppler Velocimeter Technical
906 Documentation.

907 Soulsby, R., 1993. Wave-current interaction within and outside the bottom
908 boundary layer. Coastal Engineering 21 (1-3), 41–69.

909 Souza, A., Bolaños, R., Wolf, J., Prandle, D., 2011. Measurement Tech-
910 nologies: Measure What, Where, Why, and How? Vol. 2 of Treatise on
911 Estuarine and Coastal Science. Waltham: Academic Press., pp. 361-394.

912 Souza, A. J., Lane, A., 2013. Effects of freshwater inflow on sediment trans-
913 port. Journal of Operational Oceanography 6 (1), 27–31.

914 Stanev, E., Wolff, O., Brink-Spalink, G., 2006. On the sensitivity of the
915 sedimentary system in the East Frisian Wadden Sea to sea-level rise
916 and wave-induced bed shear stress. Ocean Dynamics 56, 266–283, dOI
917 10.1007/s10236-006-0061-6.

918 Strom, K., Keyvani, A., 2011. An explicit full-range settling velocity equa-
919 tion for mud flocs. Journal of Sedimentary Research 81, 921–934, dOI:
920 10.2110/jsr.2011.62.

921 Tennekes, H., Lumley, J., 1972. A First Course in Turbulence. The Mas-
922 sachusetts Institute of Technology.

923 Thurston, W., 2009. Turbulence as a mediator of processes in a macrotidal
924 estuary. Ph.D. thesis, University of Leeds, School of Earth and Environ-
925 ment, Leeds, UK.

926 Todd, D., 2014. Temporal variability of suspended particulate matter in a
927 tidal estuary. Ph.D. thesis, University of Bangor, Bangor, UK.

928 Trowbridge, J., 1998. On a technique for measurement of turbulent shear
929 stress in the presence of surface waves. Journal of Athmospheric and Ocean
930 Technology 15 (1), 290–298.

931 Turner, A., Millward, G., Tyler, A., 1994. The distribution and chemical
932 composition of particles in a macrotidal estuary. Estuarine, Coastal and
933 Shelf Science 38, 1–17.

934 van Leussen, W., 1994. Estuarine macroflocs and their role in fine-grained
935 sediment transport. Ph.D. thesis, University of Utrecht, The Netherlands.

936 van Leussen, W., 1999. The variability of settling velocities of suspended fine-
937 grained sediment in the Ems estuary. Journal of Sea Research 41, 109–118.

938 Verney, R., Lafite, R., Brun-Cottan, J., Le Hir, P., 2011. Behaviour of a floc
939 population during a tidal cycle: laboratory experiments and numerical
940 modelling. Continental Shelf Research 31, S64–S83.

941 Voulgaris, G., Trowbridge, J., 1998. Evaluation of the acoustic doppler ve-
942 locimeter (adv) for turbulence measurements. Journal of Atmospheric and
943 Ocean Technology 15 (1), 272–289.

944 Wang, Y., Voulgaris, G., Li, Y., Yang, Y., Gao, J., Chen, J., Gao, S., 2013.
945 Sediment resuspension, flocculation, and settling in a macrotidal estuary.
946 Journal of Geophysical Research 118, 5591–5608, i:10.1002/jgrc.20340.

947 Wiberg, P., Sherwood, C., 2008. Calculating wave-generated bottom orbital
948 velocities from surface-wave parameters. Computers & Geosciences 34,
949 1243–1262, doi:10.1016/j.cageo.2008.02.010.

950 Winterwerp, J. C., 1998. A simple model for turbulence induced flocculation
951 of cohesive sediment. Journal of Hydraulic Research 36, 309–326.

952 Winterwerp, J. C., 2002. On the flocculation and settling velocity of estuarine
953 mud. Continental Shelf Research 22, 1339–1360.

954 Winterwerp, J. C., Manning, A. J., Martens, C., de Mulder, T., Vanlede, J.,
955 2006. A heuristic formula for turbulence-induced flocculation of cohesive
956 sediment. Estuarine, Coastal and Shelf Science 68, 195–207.

957 Winterwerp, J. C., van Kesteren, W. G. M., 2004. Introduction to the physics
958 of cohesive sediment in the marine environment, 1st Edition. Elsevier, B.
959 V., Amsterdam, The Netherlands.

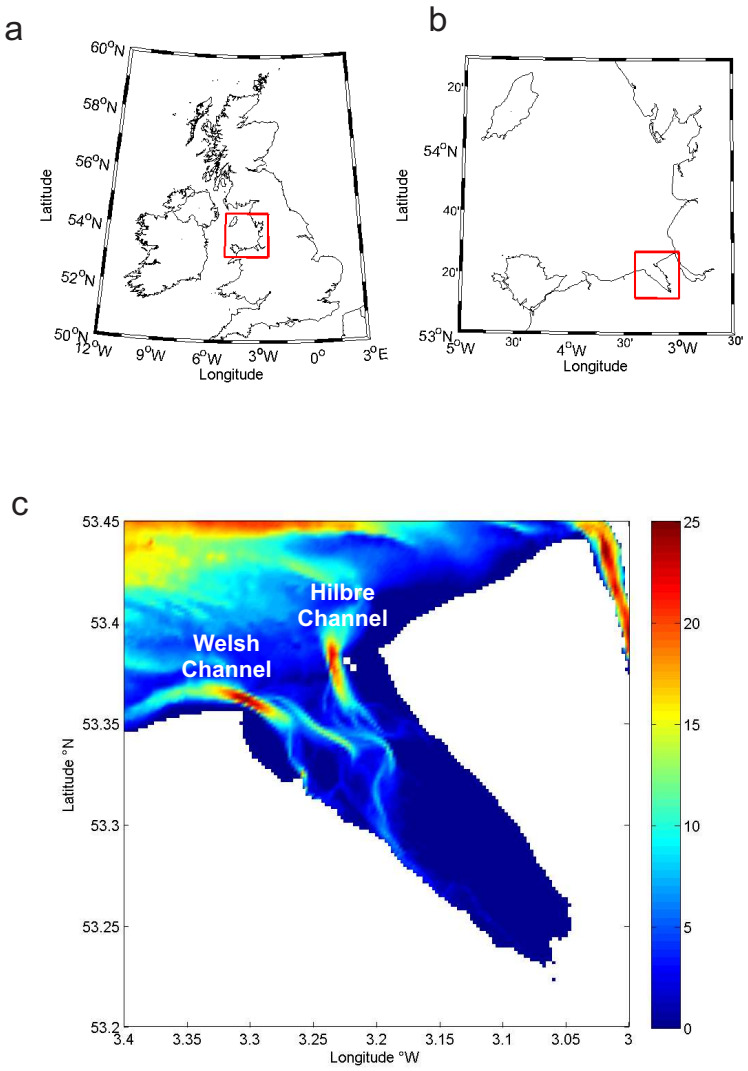

Figure 1: Location of the study site. a) United Kingdom, Liverpool Bay in red square, b) Liverpool Bay with the Dee Estuary in red square, and c) Dee Estuary, channels, Welsh to the west and Hilbre to the east of the entrance, and depth in metres.

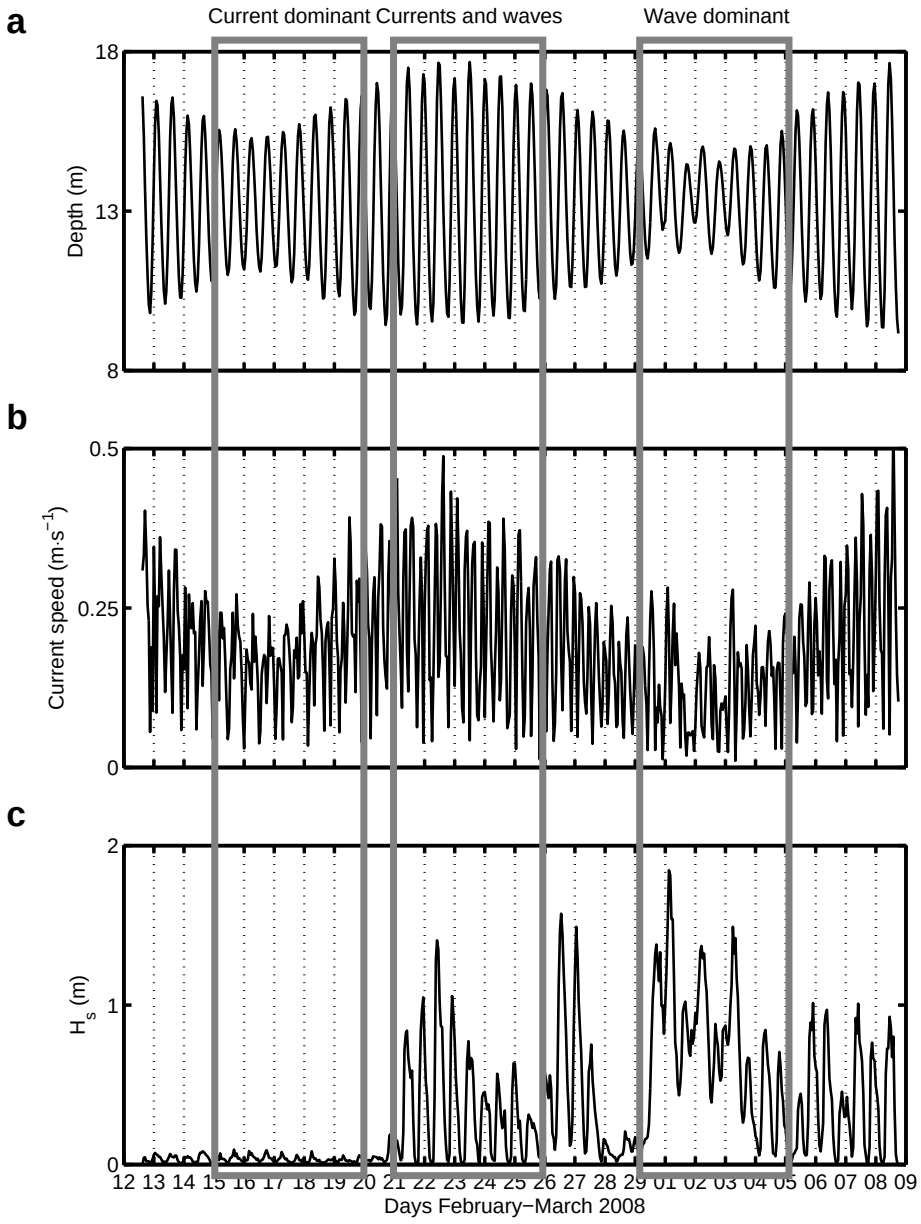

Figure 2: Separation of observations into three hydrodynamic regimes marked with grey rectangles. a) Water depth, b) horizontal bed current speed, c) significant wave height H_s.

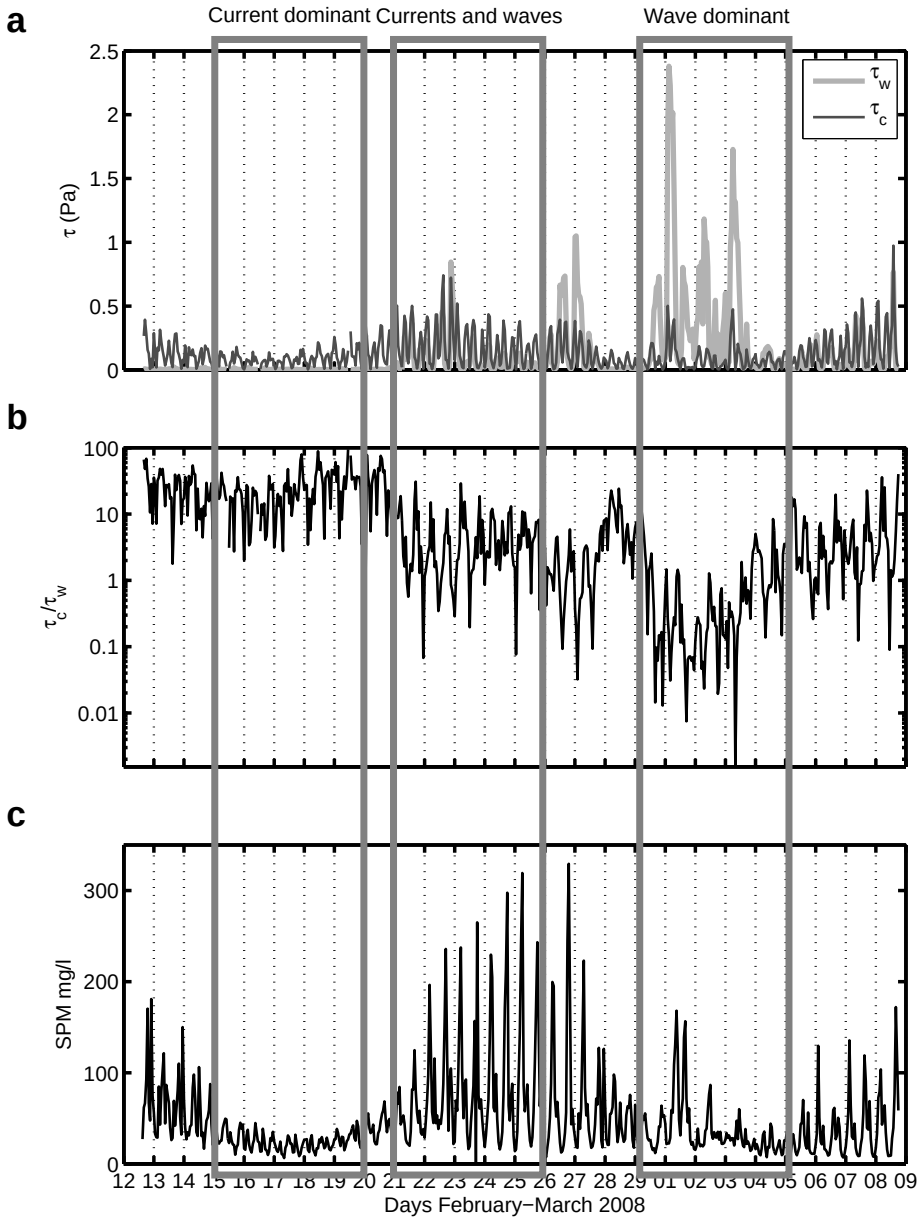

Figure 3: Shear stresses and suspended sediments during the three regimes. a) Shear stresses from currents τ_c and waves τ_w, b) ratio between τ_c and τ_w, and c) suspended particulate matter concentration.

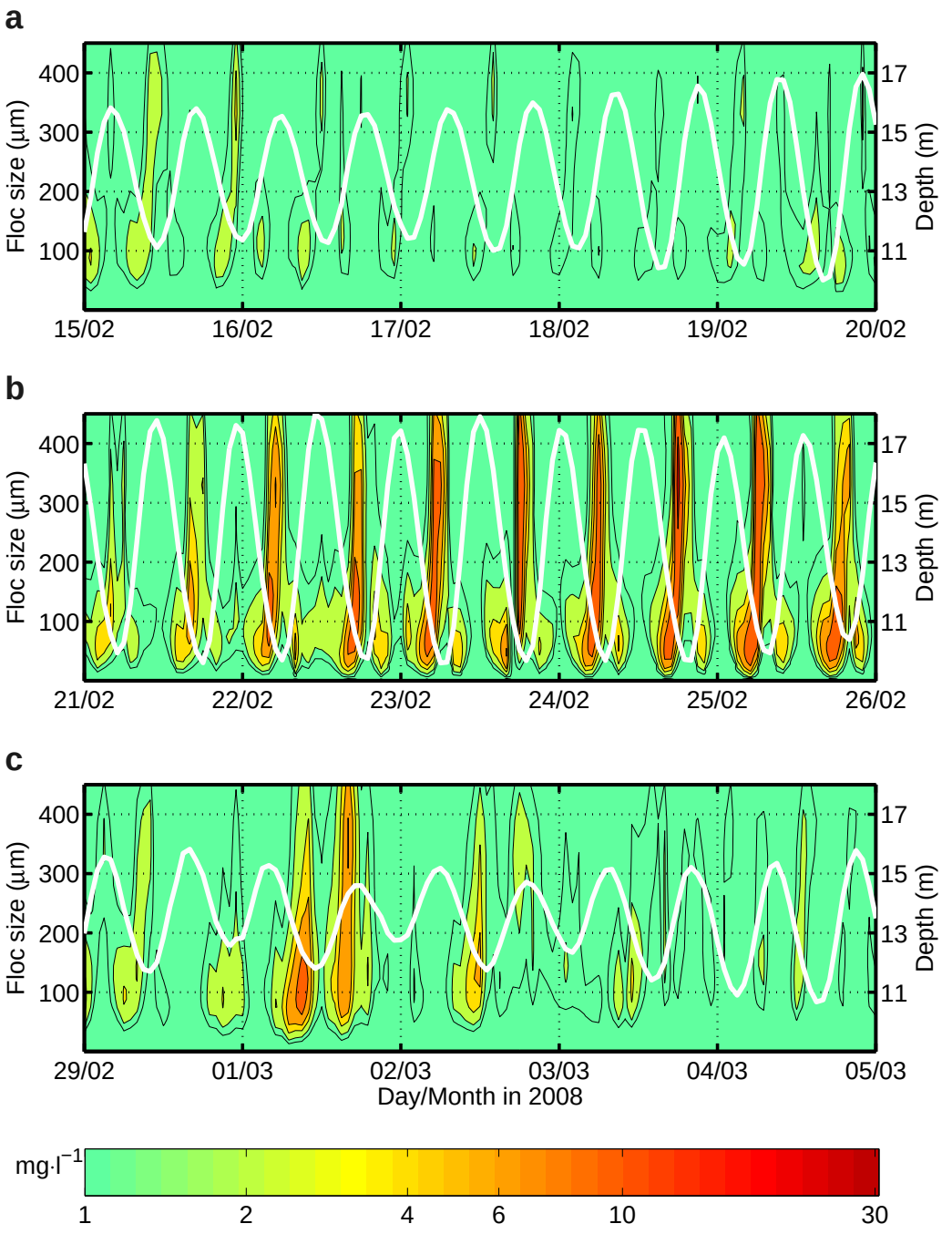

Figure 4: Floc size spectrum for the three regimes as measured by the LISST and water depth (white line). a) "current-dominant" regime, b) "currents-waves" regime, and c) "wave-dominant" regime.

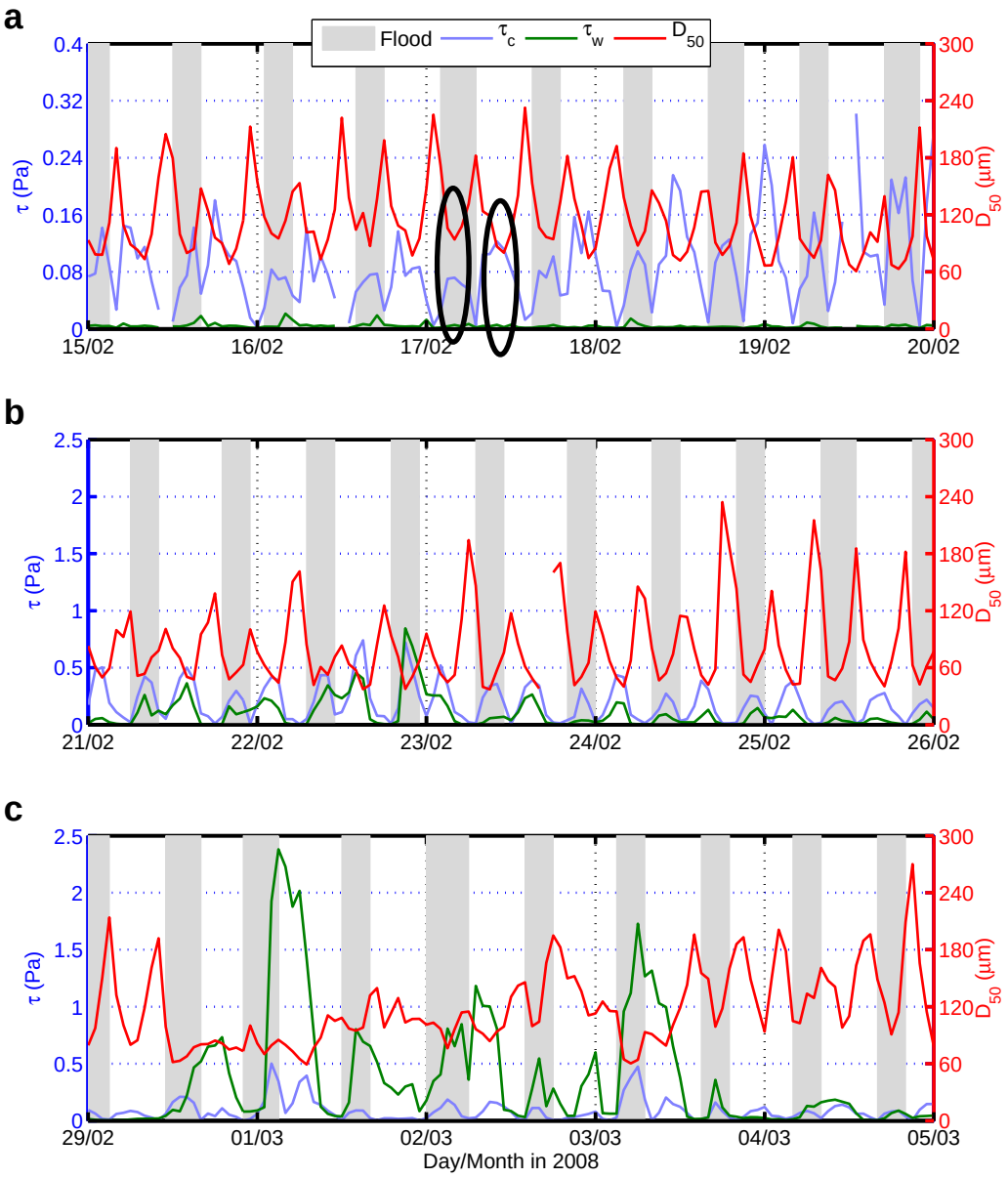

Figure 5: Shear stress from currents (τ_c), waves (τ_w), and median floc sizes (D_{50}) for each hydrodynamic regime: a) "current-dominant", ellipses denote an example of asymetries in shear stress maxima and floc size minima, b) "currents-waves" and c) "wave-dominant". Note the change in shear stress vertical scale in (a).

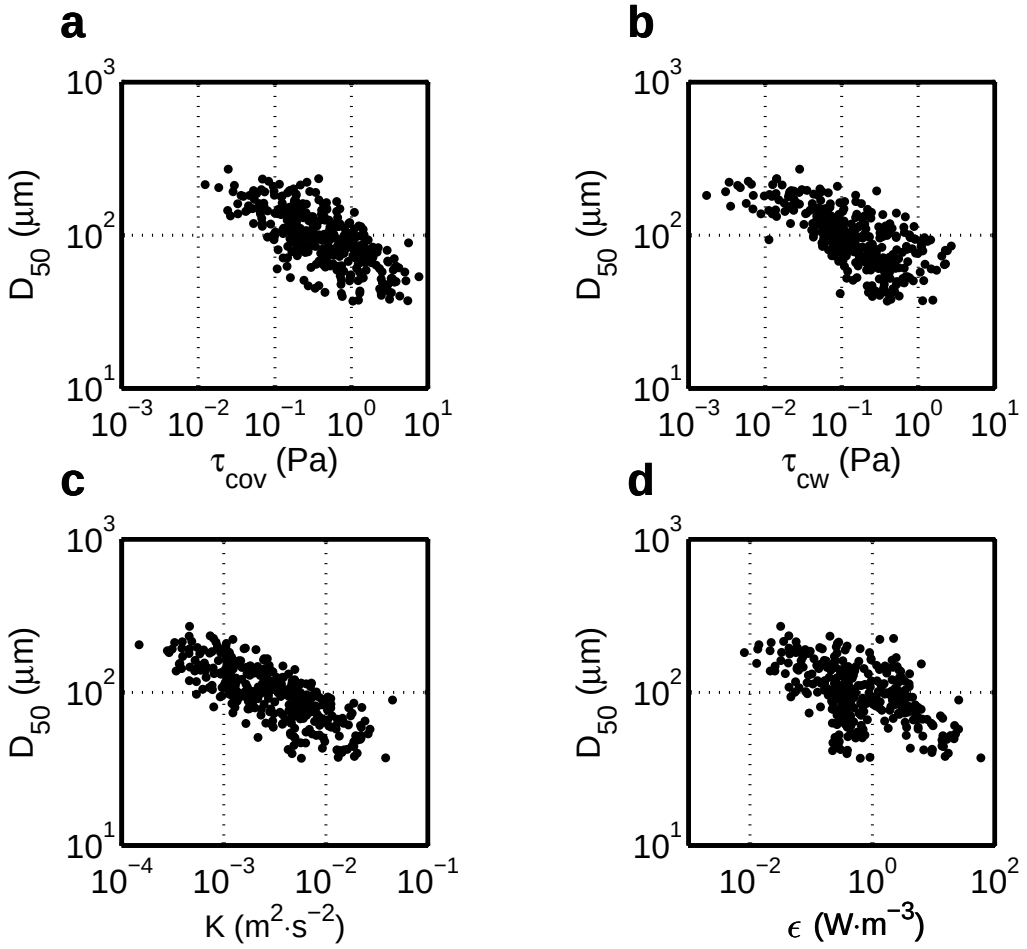

Figure 6: Dispersion diagram comparison showing the relationship of different turbulent variables with median floc size (D_{50}) for the entire data set: a) turbulent stress using the covariance method (τ_{cov}), b) maximum bed shear stress from the currents and waves analysis (τ_{cw}), c) effective kinetic energy (K) values from Reynolds decomposition of the current velocity record, and d) dissipation of turbulent kinetic energy (ϵ) from the turbulent spectrum analysis.

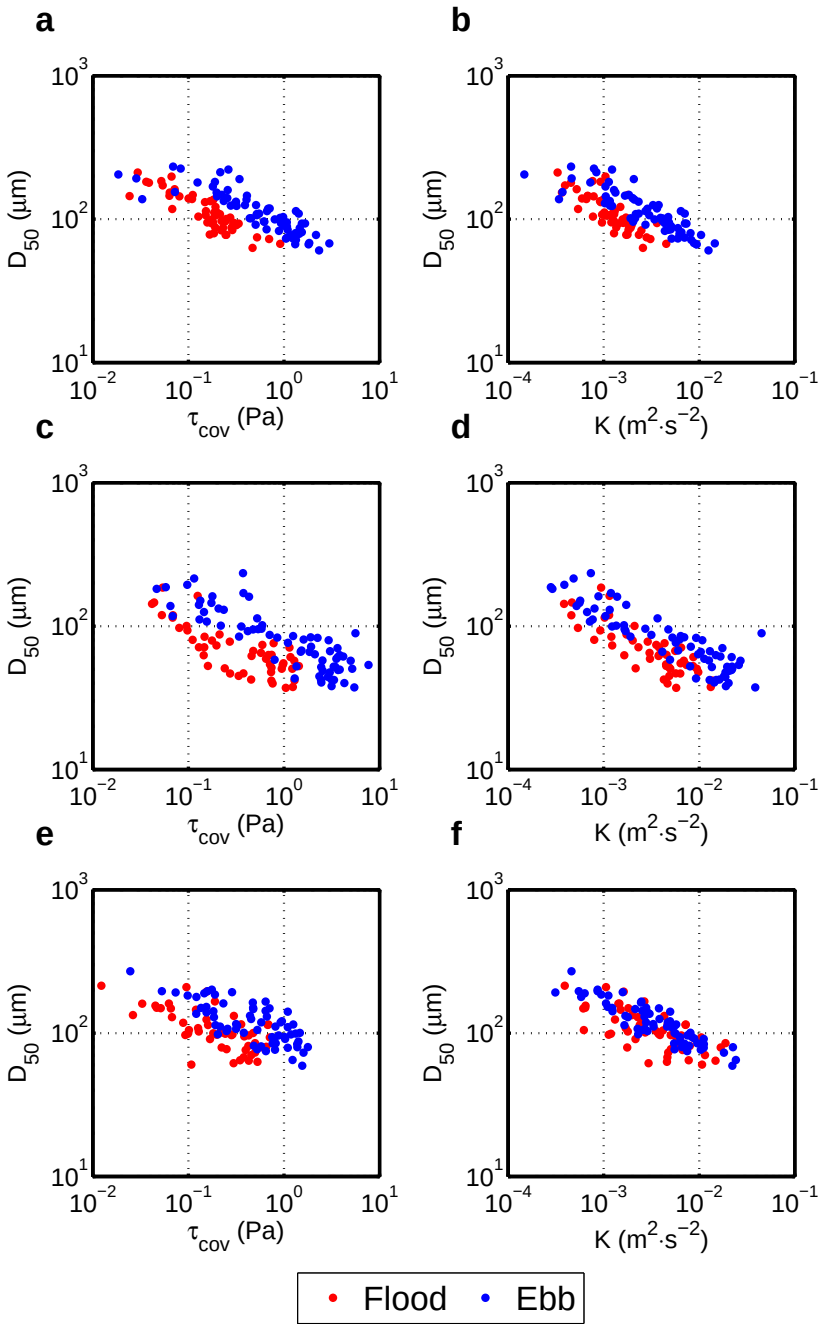

Figure 7: Median floc size as a function of shear stress from the covariance method τ_{cov} and K for the three regimes and tidal phases: a) and b) "current-dominant", c) and d) "currents-waves", e) and f) "wave-dominant".

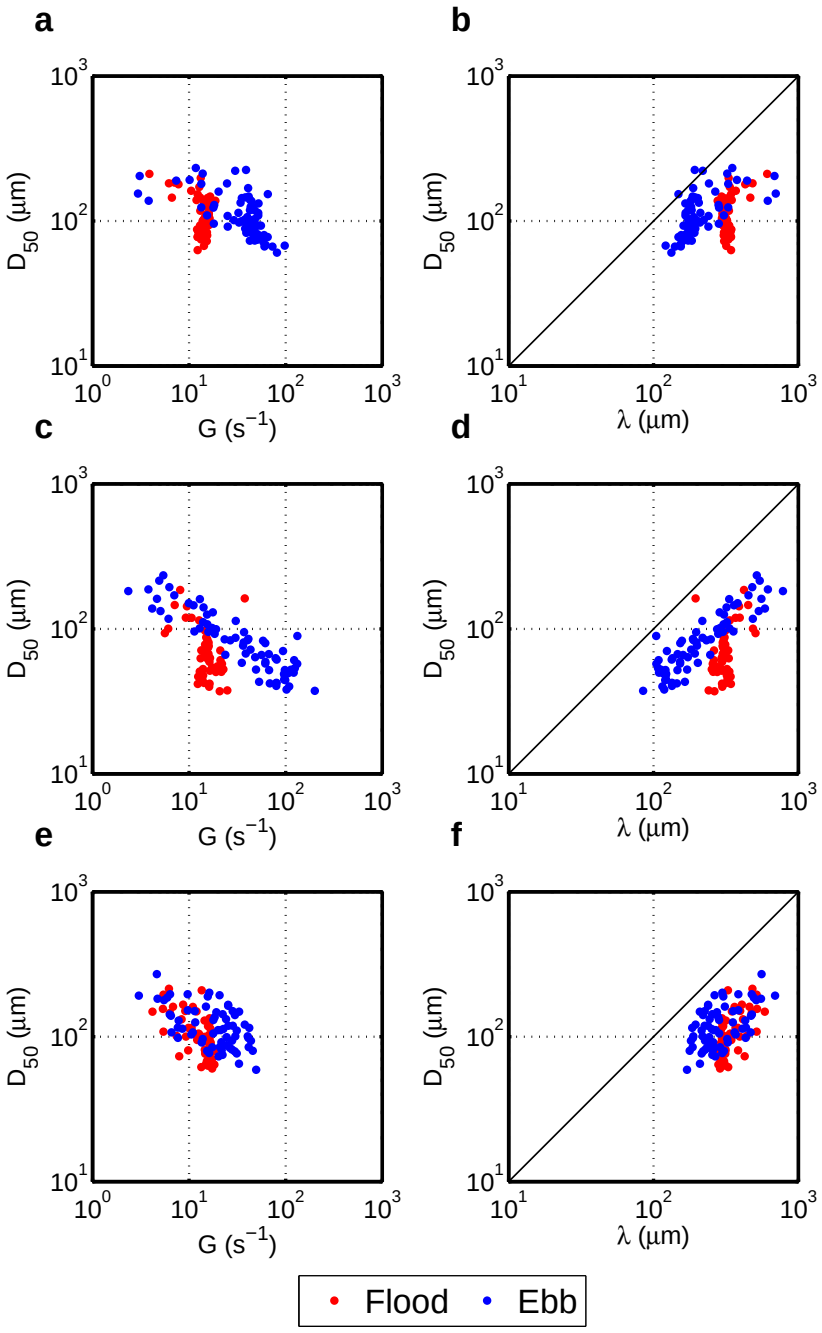

Figure 8: Median floc size D_{50} against turbulent shear rate G and Kolmogorov microscale λ for the three regimes and tidal phases: a) and b) "current-dominant", c) and d) "currents-waves", e) and f) "wave-dominant".

Table 1: Comparison of coefficients resulting of curve fittings of the forms $D_{50}=A\cdot(K)^B$ and $D_{50}=A\cdot(\tau_{cov})^B$ to distributions in figure 7. R^2: determination coefficient. RMSE: Root Mean Square Error.

		K			τ_{cov}		
		Flood	Ebb	Flood and Ebb	Flood	Ebb	Flood and Ebb
Current dominant	A	7.06	18.33	21.89	59.14	93.37	87.21
	B	-0.41	-0.31	-0.26	-0.34	-0.27	-0.20
	R^2	0.66	0.75	0.55	0.77	0.73	0.51
	RMSE	113.3	116.4	113.9	113.7	115.6	113.2
Currents - waves	A	8.97	15.46	14.56	48.87	78.31	66.44
	B	-0.35	-0.31	-0.29	-0.29	-0.30	-0.23
	R^2	0.70	0.80	0.67	0.63	0.73	0.48
	RMSE	71.2	87.0	79.3	70.2	84.5	76.47
Wave dominant	A	26.10	21.65	23.71	71.57	94.72	89.82
	B	-0.24	-0.30	-0.27	-0.23	-0.26	-0.18
	R^2	0.47	0.81	0.62	0.44	0.55	0.32
	RMSE	106.8	121.5	114.6	106.5	119.4	112.4
All data	A	17.81			77.68		
	B	-0.29			-0.24		
	R^2	0.58			0.48		
	RMSE	101.9			100.3		

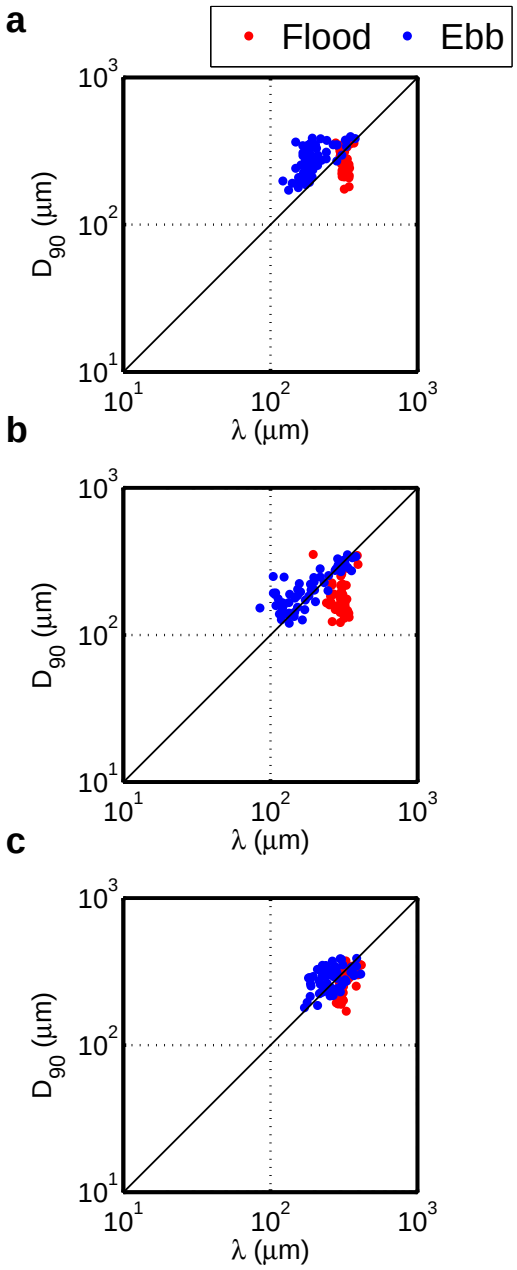

Figure 9: Kolmogorov microscale λ and D_{90} relationships for the three regimes and tidal phases: a) "current-dominant", b) "currents-waves", and c) "wave-dominant". Axes scaling have been kept as in figure 8 for comparison.

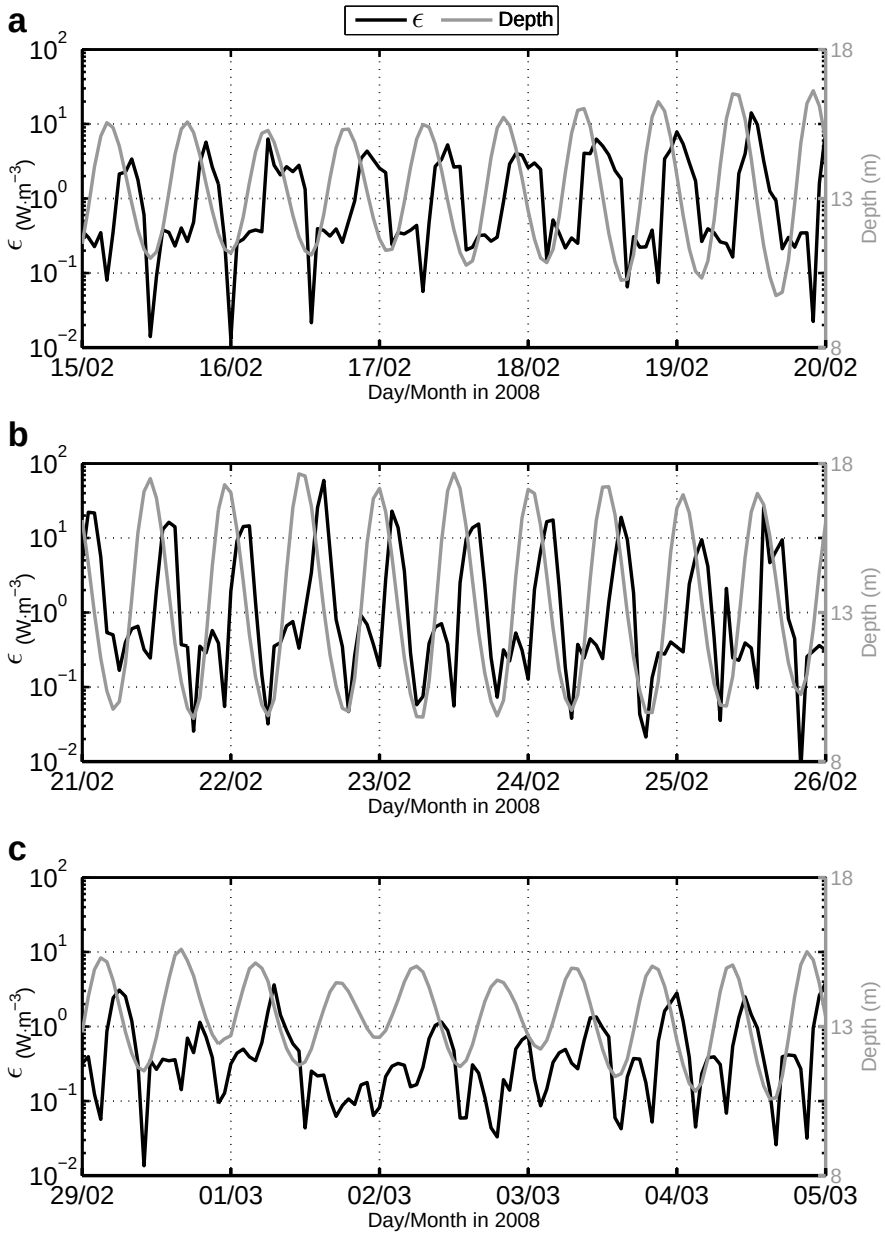

Figure 10: Time series of dissipation of turbulent kinetic energy ϵ for the three regimes: a)"current dominant", b) "currents-waves", and c) "wave-dominant".

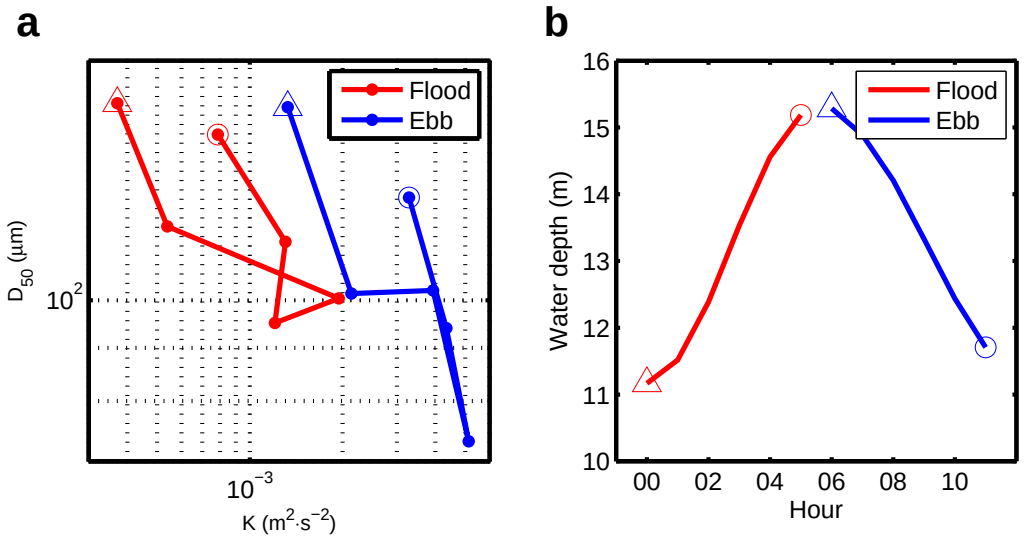

Figure 11: a) Hysteresis effect in the relationship between K and median floc size during a tidal cycle on 16 February 2008, and b) corresponding depth during the tidal cycle. Triangles and circles mark the start and end of each phase, respectively.